Journal of Power Sources 198 (2012) 14–22

Contents lists available at SciVerse ScienceDirect

Journal of Power Sources

journal homepage: www.elsevier.com/locate/jpowsour

Preparation of core (Ni base)–shell (Silicalite-1) catalysts and their application for alkali resistance in direct internal reforming molten carbonate fuel cell

Jian Zhang[a], Xiongfu Zhang[a,*], Min Tu[a], Weifeng Liu[a,b], Haiou Liu[a], Jieshan Qiu[a,**], Li Zhou[b], Zhigang Shao[b], Hung Lai Ho[c], King Lun Yeung[c]

[a] State Key Laboratory of Fine Chemicals, School of Chemical Engineering, Dalian University of Technology, Dalian 116024, PR China
[b] Fuel Cell Research & Development Center, Dalian Institute of Chemical Physics, Dalian 116023, PR China
[c] Department of Chemical and Biomolecular Engineering, the Hong Kong University of Science and Technology, Clear Water Bay, Kowloon, Hong Kong, SAR, PR China

ARTICLE INFO

Article history:
Received 4 July 2011
Received in revised form
21 September 2011
Accepted 22 September 2011
Available online 29 September 2011

Keywords:
Fuel cell
Zeolite membrane
Core–shell catalyst
Methane steam reforming
Catalyst deactivation

ABSTRACT

Alkali-resistant Ni/SiO_2–Sil-1 and Ni/Al_2O_3–Sil-1 core–shell catalysts were prepared for use in direct internal reforming molten carbonate fuel cell (DIR-MCFC). A thin zeolite shell was grown on the surface of catalyst beads to create a diffusion barrier against alkali poisons in the vapors generated from the electrolyte during DIR-MCFC operation. The synthesis of low defect zeolite shell was investigated and the effects of shell thickness on catalyst activity were examined. A mathematical model of the reaction and alkali-poisoning was developed and the optimum zeolite shell thickness was determined. The experimental and modeling results demonstrated that the core–shell catalyst is more resistant to alkali poisoning and a zeolite shell thickness of 3.5 μm can protect the catalyst for at least 100 h following a failure of the anode barrier in DIR-MCFC to give sufficient time for repair.

1. Introduction

Driven by the growing demand for cleaner and more efficient power generation, the molten carbonate fuel cells (MCFC) have attracted significant interests from governments and industries [1]. Important advances in materials and cell construction [2] contribute to the development and refinement of direct internal reforming (DIR) MCFC. The DIR-MCFC can achieve higher efficiency (up to 14% higher) and has lower capital and operating cost through coupling of the endothermic steam reforming reaction and the exothermic electrochemical conversion at the anode [3,4]. In addition, DIR-MCFC has better water management, greater fuel flexibility as well as lower greenhouse gas emission [5].

The high working temperatures (≥900 K) and elevated alkali content of the electrolyte (i.e., $62Li_2CO_3$:$38K_2CO_3$) are detrimental to the reforming catalyst of DIR-MCFC [6,7]. In particular, the alkalis poison the catalyst and researches show that alkalis in the electrolyte can reach the catalyst by liquid creep or vapor [8]. This can be prevented by separating the catalyst and the anode chamber with ceramic barriers [9,10] and metal foils [11]. There are also significant efforts in developing alkali-resistant catalysts including Ru/ZrO_2 [12] and Ni catalysts supported on alkali-resistant γ-$LiAlO_2$ [13], MgO–TiO_2 [14] and MgO–Al_2O_3 [15]. A nonuniform catalyst distribution can also ameliorate the effects of poisons by locating the catalysts in an interior location of the pellet [16–19].

This study investigates a core–shell catalyst consisting of a core nickel catalyst (i.e., Ni/SiO_2 and Ni/Al_2O_3 beads) with a pure silica Sil-1 zeolite shell. The shell acts as a transport barrier for the alkali vapor and electrolyte solution to protect the catalyst from rapid poisoning. Core–shell catalyst with zeolite shell had been used as selective separation layer by Tsubaki et al. [20] in Fischer-Tropsch synthesis (FTS) reaction using a Co/SiO_2 core with ZSM-5 shell and by Kapteijn et al. [21] for selective hydrogenation of 1-hexene from a mixture containing 3,3-dimethylbut-1-ene (3,3-DMB) with a Co/TiO_2 catalyst with Sil-1 shell. Both research groups showed that selective transport across the zeolite shell is responsible for the enhanced selectivity to the target product. Zeolites are also effective barrier against contamination from support materials in Pd membranes [22–24] and can simultaneously serve as catalyst for reactions [25]. Our prior work shows that a core–shell, Ni/Al_2O_3–Sil-1 catalyst can tolerate the high alkali concentration generated in DIR-MCFC [26]. It is the purpose of this study to determine the optimum zeolite shell thickness for a core–shell catalyst designed to survive at least 100 h operation under high alkali

* Corresponding author. Tel.: +86 411 84986155; fax: +86 411 84986155.
** Corresponding author. Tel.: +86 411 84986080; fax: +86 411 84986080.
E-mail addresses: xfzhang@dlut.edu.cn (X. Zhang), jqiu@dlut.edu.cn (J. Qiu).

0378-7753/$ – see front matter © 2011 Elsevier B.V. All rights reserved.
doi:10.1016/j.jpowsour.2011.09.070

Nomenclature

a	specific interfacial area (m^{-1})
f	fraction of the poison adsorbed catalytic site to the total catalytic side (–)
k^{ad}	adsorption rate constant ($m^3\ mol^{-1}\ s^{-1}$)
t	time (s)
$\dot{v}$	volumetric flowrate ($m^3\ s^{-1}$)
β	proportionality constant (–)
C	volume concentration ($mol\ m^{-3}$)
D	diffusivity ($m^2\ s^{-1}$)
D'	modified diffusivity ($m\ kg^{-1}$)
F	molar flowrate ($mol\ s^{-1}$)
K	equilibrium constant between the pore and bulk gas phases (–)
K'	modified equilibrium constant between the pore and bulk gas phases (s^{-1})
W	weight (kg)
ρ	apparent density ($kg\ m^{-3}$)
δ	thickness of Silicalite-1 shell membrane (m)
θ	surface concentration ($mol\ m^{-2}$)

Subscripts

CH_4	methane
P	Poison
P·S	Poison-adsorbed catalytic site
b	bulk gas phase
o	overall
p	catalyst pore phase
to	initial total catalytic site
t	total catalytic site
Al	alumina
Sil-1	Silicalite-1
Cat	catalyst

conditions following a simulated failure of the anode barrier in a DIR-MCFC.

2. Experimental

2.1. Preparation of core–shell nickel reforming catalyst

2.1.1. Preparation of core nickel catalysts

CARIACT Q-10 silica beads (0.8–1.7 mm diameter, average pore volume of 0.99 $cm^3\ g^{-1}$ and BET surface area of 300 $m^2\ g^{-1}$) from Fuji Silysia Chemical Ltd. and γ-Al_2O_3 beads (0.8–2.2 mm diameter, pore volume of 0.40 $cm^3\ g^{-1}$ and BET surface area of ca. 280 $m^2\ g^{-1}$) from Dalian Haixin Chemical Ltd. were rinsed in deionized distilled water and alcohol before calcination in air for 5 h at 523 K. The nickel catalysts (12.5 wt.% Ni) were prepared by incipient wetness method from nickel nitrate solution ($Ni(NO_3)_2{\cdot}6H_2O$, 98%, Kermel). The impregnated catalyst beads were dried 12 h at 373 K, followed by air calcination at 923 K for 4 h to decompose the salt to nickel oxides.

2.1.2. Preparation of Sil-1 zeolite shell

A low defect zeolite shell was deposited on the beads using procedures borrowed from zeolite membrane preparation [27–29]. The catalyst beads were seeded with a layer of Sil-1 zeolite seeds prepared according to synthesis procedure reported in previous works [30–32]. Seeding minimizes the effects of support chemistry and promotes zeolite deposition and growth [33]. Seeds can influence the zeolite growth and film orientation [34], and prior works showed that 160 nm Sil-1 seeds are optimum for core–shell catalyst preparation [26,35]. The Sil-1 seeds were obtained after 18 h of hydrothermal synthesis at 368 K of a clear synthesis solution with a molar composition of $1TPA_2O{:}8SiO_2{:}216H_2O$. The tetrapropylammonium hydroxide (TPAOH, 25%) was purchased from Zhejiang Kente Chemical Co., Ltd. and the silica precursor tetraethyl orthosilicate (TEOS, 98%) was supplied by Kermel. The seeds were recovered by a series of centrifugation and washing steps and a 0.08 wt.% Sil-1 seed suspension in ethanol was prepared.

The catalyst beads were seeded by first grafting a layer of 3-aminopropyltrimethoxysilane (APTMS, Aldrich) on the beads as organic linker, followed by the deposition of Sil-1 seeds. The excess seeds were washed away with ethanol before drying at 353 K for 12 h and air calcination at 823 K for another 12 h. A layer of zeolite shell was grown on the seeded beads by hydrothermal regrowth. The synthesis composition and conditions can affect the zeolite growth, morphology and orientation, and ultimately the molecular transport across the zeolite shell [36–38]. The zeolite shell was deposited from a synthesis mixture containing $1TPA_2O{:}8SiO_2{:}2400H_2O$, and different shell thicknesses were obtained by controlling the synthesis temperature and time. The resulting core–shell catalysts were calcined in air at 923 K for 4 h to remove the organic structure directing molecule, TPA^+ from the zeolite pores.

2.1.3. Catalyst characterization

The appearance of the catalyst beads were observed at 6× magnification and captured with a digital camera (Canon A760). The beads were halved with a clean blade and mounted on a holder for examination under scanning electron microscope (SEM, JSM-6360LV). The samples were sputter-coated with gold to prevent sample charging. An elemental mapping by energy dispersive X-ray spectroscopy (EDXS, JED 2300) was done in situ during SEM imaging. Elemental analysis was done on 5 mg dissolved catalyst samples using an inductively coupled plasma, atomic emission spectrometer (ICP AES, Optima 2000DV).

2.2. Alkali-resistance of core–shell catalysts for methane steam reforming

An out-of-cell test (OCT) was used to investigate the alkali resistance of the core–shell catalysts. This provides more accurate reaction data and avoids complication from cell operation. In the out-of-cell test, the catalysts were exposed to the alkali vapor for a fixed period of time before conducting the methane reforming reaction. The core–shell catalysts and the reference catalysts, Ni/SiO_2 and Ni/Al_2O_3 were reduced in hydrogen at 923 K for 5 h before the reaction study.

The catalysts were exposed to alkali vapor generated by bubbling nitrogen gas through 4 g of electrolytes (i.e., 62 mol% Li_2CO_3 and 38 mol% K_2CO_3) in a stainless steel reactor (30 mm ID) as shown in Fig. 1a. 1.2 g catalyst beads were placed on a perforated holder above the electrolyte. The treatment was carried out at 923 K same as the operating temperature in DIR-MCFC. The catalysts were treated for a fixed length of time ranging from 5 to 100 h. The amount of electrolyte evaporated and the catalyst weight gain were recorded. Treated catalysts were also examined by SEM, EDXS and analyzed by ICP-AES before methane steam reforming reaction. The steam reforming reaction was carried out in a separate reactor that has a diameter of 8 mm and a length of 400 mm (Fig. 1b). The 0.8 g catalyst was treated for 5 h in 40 sccm flowing hydrogen at 923 K before switching the flow to 20 sccm mixture of steam and methane ($H_2O/CH_4 = 3$). The reaction was carried out for 7 h and the product stream was monitored by an on-line gas chromatograph equipped with a packed column (200 mm length × 3 mm diameter, TDX-01, Shanghai Techcomp Ltd) and a thermoconductivity detector (GC

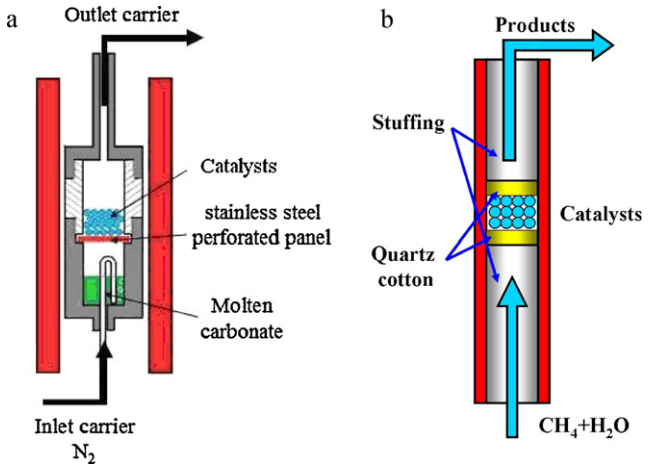

Fig. 1. Schematic drawings of reactor set-ups for (a) electrolyte vapor exposure and (b) methane steam reforming reaction.

7890T, Shanghai Techcomp Ltd). Argon was used as the carrier gas for the gas chromatograph.

2.2.1. Reaction modeling and catalyst optimization

A mathematical model was developed based on the experimental data to investigate the effects of alkali vapor on catalyst deactivation and determine the optimum zeolite shell thickness of the core–shell catalyst. A plug flow reactor was assumed for the reaction. The transport across the zeolite shell is considered the rate determining step in the reaction, thus the methane concentration in the catalyst core is negligible compared to the bulk concentration of methane in the reactant stream. Methane and alkali diffusivities through the zeolite–shell and catalyst core are isotropic with the adsorption of alkali being the rate determining step in catalyst poisoning. The adsorption rate is taken to be proportional to the alkali concentration in the catalyst pores in equilibrium with the bulk alkali. The Modified equilibrium ($K'_{P,Al}$) and proportionality (β) constants were obtained from the experimental reaction data. Summaries of the modeling equations and parameters are given in Tables 1 and 2, respectively. The model was used to examine the effects of shell thickness on the reaction and alkali poisoning, and

Table 1
Mathematical modeling equations for DIR-MCFC.

Methane reforming reaction	Catalyst deactivation
Mole balance equation for methane through catalyst bed:	Poisoning reaction:
$dF_{CH_4,b} = -k_{CH_4,o} \cdot a \cdot dW_{Cat} \cdot \frac{1}{\rho_{Cat}} \cdot (C_{CH_4,b} - C_{CH_4,p})$	$P + S \rightarrow P \cdot S$
$dF_{CH_4,b} = -k_{CH_4,o} \cdot a \cdot dW_{Cat} \cdot \frac{1}{\rho_{Cat} \cdot \dot{v}_b} \cdot F_{CH_4,b}$	Catalyst deactivation rate = Poison adsorption rate
Let $k'_{CH_4,o} = \frac{k_{CH_4,o} \cdot a}{\rho_{Cat} \cdot \dot{v}_b}$	$-\frac{d\theta_t}{dt} = \frac{d\theta_{P,S}}{dt} = k_P^{ad}(\theta_{to} - \theta_{P,S})C_{P,p}$
$\frac{dF_{CH_4,b}}{dW_{Cat}} = -k'_{CH_4,o} \cdot F_{CH_4,b}$	Let $f = \frac{\theta_{P,S}}{\theta_{to}}$
Resistance in series model:	$\therefore \frac{df}{dt} = k_P^{ad}(1-f)C_{P,p}$
$\frac{1}{k'_{CH_4,o}} = \frac{1}{k'_{CH_4,Al}} + \frac{1}{k'_{CH_4,Sil\text{-}1}}$	Assume that the poison concentration in pores was in equilibrium with that in bulk gas phase:
Where	$K_{P,o} = \frac{C_{P,p}}{C_{P,b}}$
$k'_{CH_4,Sil\text{-}1} = \frac{D'_{CH_4,Sil\text{-}1}}{\delta}$, $k'_{CH_4,Al} = \frac{D'_{CH_4,Al}}{\delta}$	$\therefore \frac{df}{dt} = k_P^{ad}(1-f)K_{P,o}C_{P,b}$
Modified mass transfer coefficient and diffusivity:	Where the overall equilibrium constant $K_{P,o}$ was calculated using resistance in series method:
$k'_{CH_4,Sil-1} = \frac{k_{CH_4,Sil\text{-}1} \cdot a}{\rho_{Cat} \cdot \dot{v}_b}$, $k'_{CH_4,Al} = \frac{k_{CH_4,Al} \cdot a}{\rho_{Cat} \cdot \dot{v}_b}$	$\frac{1}{K_{P,o}} = \frac{1}{K_{P,Al}} + \frac{1}{K_{P,Sil-1}}$
$D'_{CH_4,Sil-1} = \frac{D_{CH_4,Sil\text{-}1} \cdot a}{\rho_{Cat} \cdot \dot{v}_b}$, $D'_{CH_4,Al} = \frac{D_{CH_4,Al} \cdot a}{\rho_{Cat} \cdot \dot{v}_b}$	It was assumed that equilibrium constant for Silicalite-1 membrane was inversely proportional to the shell-thickness:
	$K_{P,Sil-1} \propto \frac{1}{\delta}$
	$\therefore K_{P,Sil-1} = \frac{\beta}{\delta}$, where β is proportionality constant
	Let $K'_{P,o} = k_P^{ad} K_{P,o} C_{P,b}$
	$\therefore \frac{df}{dt} = K'_{P,o}(1-f)$
	By integrating the equation on both sides:
	$\ln(1-f) = -K'_{P,o}t$
	$f = 1 - e^{-k_{P,o}^{ad} t}$

Table 2
Numerical values of modeling parameters.

Parameters	Symbol	Value	Unit
Gas volumetric feed rate	$\dot{v}$	3.33×10^{-6}	$m^3\,s^{-1}$
Temperature	T	923	K
Pressure	P	101,325	Pa
Steam to carbon molar feed ratio	$y_{CH_4,o}$	3	–
Methane molar feed rate	$F_{CH_4,o}$	4.40×10^{-6}	$mol\,s^{-1}$
Catalyst mass	m_{Cat}	0.0008	kg
Mass transfer coefficient for methane through core catalyst	$k'_{CH_4,Al}$	2314	kg^{-1}
Diffusivity of Methane through silicalite-1 shell	$D'_{CH_4,Sil-1}$	9.42×10^{-6}	$m\,kg^{-1}$
Modified equilibrium constant between bulk gas and catalyst pore for catalyst (without shell)	$K'_{P,Al}$	0.8	s^{-1}
Proportionality constant	β	2.68×10^{-4}	–

to determine the optimum shell thickness to safeguard DIR-MCFC operation during an anode barrier failure.

3. Results and discussion

3.1. Ni/MO_x–Sil-1 core–shell catalysts

The zeolite shell serves as a barrier against catalyst poisoning by the alkali electrolyte, and thus must have relatively low defect. The zeolite shell was grown on the Ni/SiO_2 and Ni/Al_2O_3 catalyst beads after seeding the beads with a layer of Sil-1 seeds. A monolayer of seeds is needed to grow a well-intergrown shell and avoid shell delamination. Uniform Sil-1 seeds of 160 ± 10 nm were attached to the surface using organic linkers. The 3-aminopropyltrimethoxysilane linkers formed a Si–O–M covalent bond with the SiO_2 and Al_2O_3, while the amino head groups interact with the hydroxyls on zeolite seeds resulting in their assembly on the bead's surface [39]. Fig. 2 shows that after calcination a monolayer of closely packed Sil-1 seeds were obtained on both Ni/SiO_2 (Fig. 2a) and Ni/Al_2O_3 beads (Fig. 2b).

Zeolite growth, microstructure and morphology are sensitive to synthesis parameters particularly temperature and time [36,37,40,41]. Scanning electron micrographs of two core–shell catalysts are shown in Fig. 3. The Sil-1 shells were grown on the Ni/SiO_2 beads following 24 h of hydrothermal regrowth at 423 and 448 K, respectively. It can be seen in Figs. 3a–c that Sil-1 shell grown at 423 K was thinner (i.e., 5 μm) and less well-intergrowth than the shell grown at 448 K (cf. Figs. 3d–f). Eight microns thick polycrystalline Sil-1 layer consisting of half micron sized crystals was deposited uniformly over the surface of the catalyst bead regrown at 448 K. A closer examination of the shell along its thickness shows that the zeolites grew with a preferred orientation along the *c*-axis consistent with Vander Drift's growth behavior [42,43]. The intergrowth within the shell extends from the surface to the barely discernable seed layer attached to the bead surface. There was no apparent delamination observed in the core–shell catalyst beads prepared in this study.

Thinner zeolite shells were obtained by simply using shorter synthesis time as shown by the cross-sections of Ni/SiO_2–Sil-1 core–shell catalysts, while longer synthesis time gave Ni/Al_2O_3–Sil-1 core–shell catalysts their thicker shells shown in Fig. 4. Sil-1 shells of 0.5, 2 and 4.5 μm were obtained for Ni/SiO_2–Sil-1 core–shell catalyst following 2, 8 and 16 h of synthesis. SEM examination shows that all the deposited zeolite shells are polycrystalline and well-intergrown. Defects were not evident from SEM analysis of the zeolite shells. The zeolite shells of the Ni/Al_2O_3–Sil-1 core–shell catalysts display similar microstructure and have measured thickness of 2.5, 5 and 6 μm following 24, 48, 72 h regrowth. The slower growth observed on the alumina beads could be explained by the presence of alumina that tends to inhibit MFI zeolite growth [44–46].

Table 3
Mass variation of alkali and catalysts during the alkali exposing test.

Catalysts	Test time (h)	Mass variations of alkali (g)*	Mass variations of catalysts (g)**
Ni/Al_2O_3–Sil-1 (3.5 μm)	5	−0.308	0.018
	10	−0.381	0.024
	20	−0.452	0.031
	60	−0.452	0.056
	100	−0.725	0.077

* 1.2 g catalysts per test.
** 4 g electrolyte ($62Li_2CO_3$:$38K_2CO_3$) per test.

Table 4
Results on Ni/Al_2O_3 and core–shell Ni/Al_2O_3–Sil-1 catalysts with different thicknesses by the alkali exposing test.

Catalysts	Shell thickness (μm)	Methane conversion (%)*	Methane conversion (%)**
Ni/Al_2O_3	0	84.1	1.3
	2.5	69.8	60.3
Ni/Al_2O_3–Sil-1	3.5	64.2	51.8
	5.4	51.1	49.0

* Fresh catalysts.
** Catalysts treated with 5 h in electrolyte vapor.

3.2. Alkali-resistance of core–shell catalysts for methane steam reforming

Ni/SiO_2 and Ni/Al_2O_3 catalysts and their corresponding core–shell catalysts were exposed to the alkali vapor generated from the molten electrolyte in the reactor set-up shown in Fig. 1a. The amount of electrolyte evaporated and the catalyst weight gain are summarized in Table 3 for the core–shell Ni/Al_2O_3–Sil-1 catalyst with 3.5 μm thick shell. The data show that longer treatment time evaporated more carbonate electrolyte with a concomitant increase in catalyst weight with exposure to the vapor. The catalysts' activities for methane steam reforming reaction were evaluated and plotted in Fig. 5. The Ni/SiO_2 and Ni/Al_2O_3 catalysts were completely poisoned after exposure to the alkali vapor and displayed low methane conversions. Both Ni/SiO_2–Sil-1 and Ni/Al_2O_3–Sil-1 core–shell catalysts are more resistant to the alkali poison and have higher methane conversions of 11% and 60%, respectively. Indeed, the core–shell catalysts display comparable conversions to the fresh catalysts. A further deactivation of Ni/SiO_2–Sil-1 in the absence of alkali poison could be attributed to catalyst sintering [39,47]. The reaction results of Ni/SiO_2–Sil-1 and Ni/Al_2O_3–Sil-1 core–shell catalysts are consistent with the report by Roh et al. [48] that alumina is a good catalyst support for nickel in steam reforming reaction.

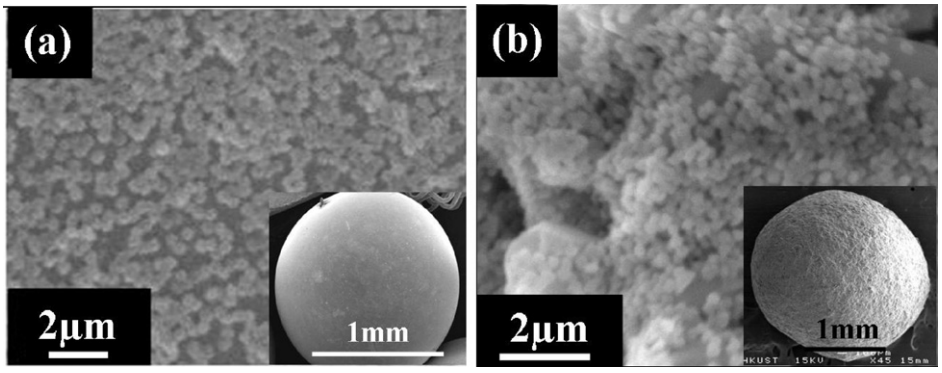

Fig. 2. SEM pictures of seeded (a) Ni/SiO_2 and (b) Ni/Al_2O_3 catalyst beads.

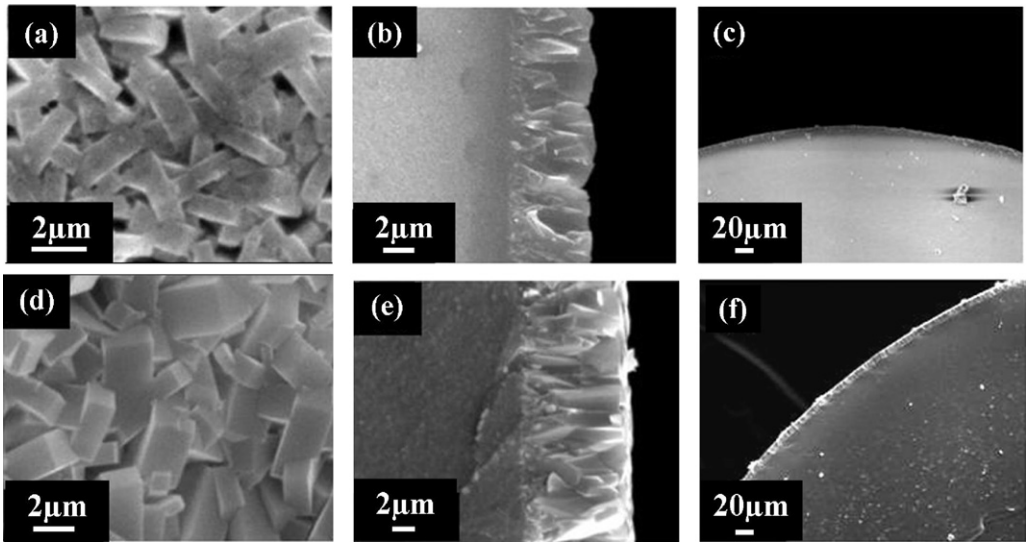

Fig. 3. SEM pictures of Ni/SiO_2–Sil-1 core–shell catalysts with shells grown for 24 h at (a–c) 423 K and (d–f) 448 K.

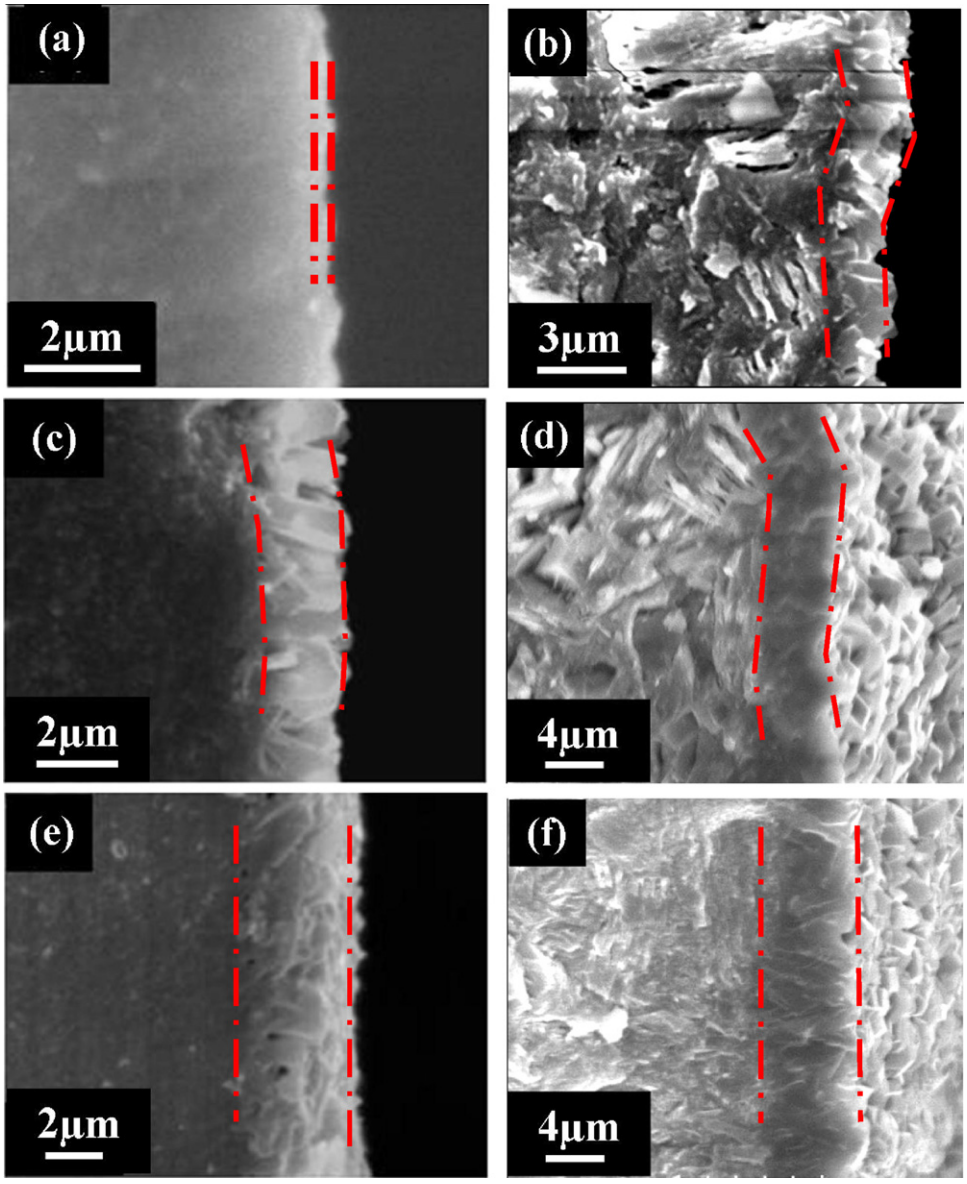

Fig. 4. SEM picture of zeolite shells grown on Ni/SiO_2 beads after (a) 2, (c) 8 and (e) 16 h, and Ni/Al_2O_3 after (b) 24, (d) 48 and (f) 72 h of zeolite regrowth.

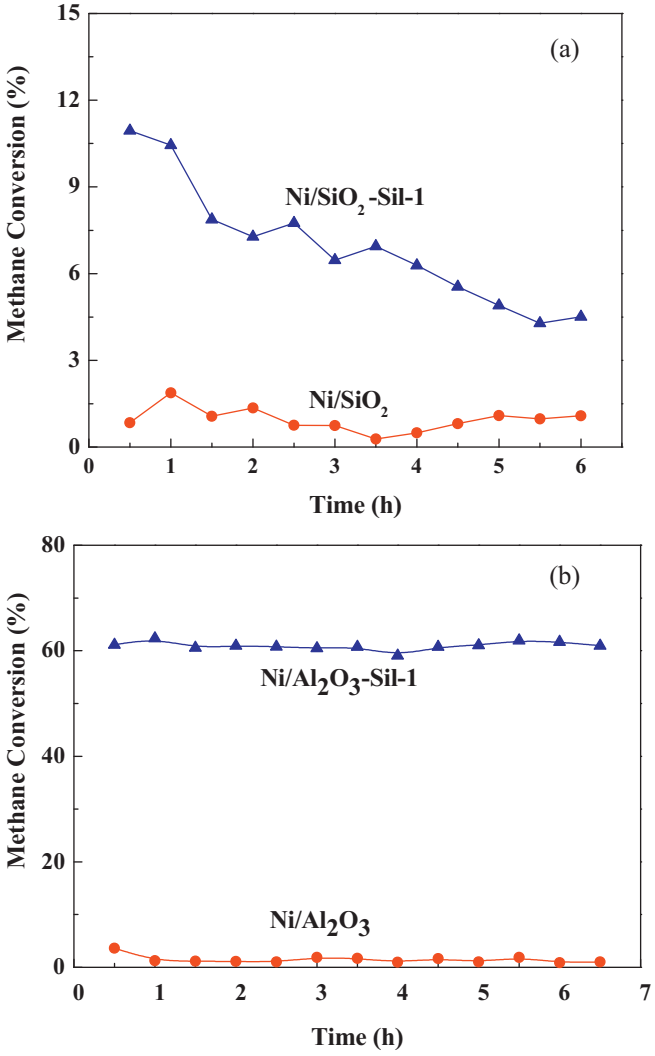

Fig. 5. Plots of methane conversion for (a) Ni/SiO_2 and Ni/SiO_2–Sil core–shell catalysts and (b) Ni/Al_2O_3 and Ni/Al_2O_3–Sil core–shell catalysts after 5 h exposure to electrolyte vapor. *Note*: the Ni/SiO_2–Sil-1 has a 3.8 μm shell and Ni/Al_2O_3–Sil-1 has 2.8 μm shell.

The methane conversions obtained from Ni/Al_2O_3 and Ni/Al_2O_3–Sil-1 catalysts before and after exposure to the electrolyte vapor for 5 h are summarized in Table 4. A methane conversion of 83% was obtained from the fresh Ni/Al_2O_3 catalyst and deposition of 2.5, 3.5 and 5.4 μm zeolite shell leads to lower conversions of ca. 70, 64 and 51%, respectively. This is due to the higher transport resistance across the zeolite shells and the calculated methane diffusivity of 10^{-5} m kg^{-1} through the zeolite shell is comparable to that reported for zeolite membranes [49,50]. Ni/Al_2O_3 was inactive after exposure to the electrolyte vapor and has a low methane conversion of 1.3% [13]. The table indicates that the zeolite shell ameliorates the poisoning of the nickel catalyst with thicker shells being more effective. The Ni/Al_2O_3–Sil-1 catalysts with shell thickness of 2.5, 3.5 and 5.4 μm gave respectively methane conversions of 60, 52 and 49% (cf. Table 4) that are 10, 12 and 2% lower than the conversions obtained before exposure to the electrolyte vapor.

The stability of Ni/Al_2O_3 catalyst and Ni/Al_2O_3–Sil-1 core–shell catalyst to long-term exposure to electrolyte vapor is plotted in Fig. 6. The catalysts were exposed to the electrolyte vapor for 5, 10, 20, 40, 80 and 100 h before performing the methane steam reforming reaction. It is clear from the results that the deposition of a thin

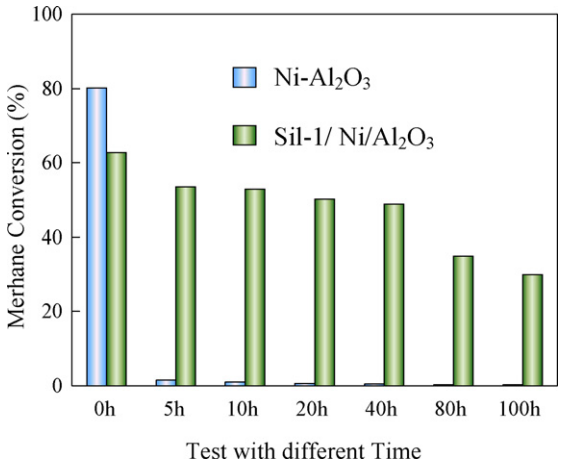

Fig. 6. Methane conversion over Ni/Al_2O_3 and Ni/Al_2O_3–Sil-1 (3.5 μm) catalysts after different time exposure to high concentration of electrolyte vapor. (For interpretation of the references to color in this figure, the reader is referred to the web version of the article.)

3.5 μm zeolite shell on Ni/Al_2O_3 catalyst made it resistant to poisoning from exposure to electrolyte vapor at high temperatures. On the other hand, Ni/Al_2O_3 catalyst was completely poisoned after 5 h exposure and is inactive to the reaction.

The Ni/Al_2O_3–Sil-1 core–shell catalyst was also subjected to tests at a lower vapor concentration that more closely mimics the real situation in DIR-MCFC. This was accomplished by placing the catalyst downstream from 5 g of alumina pellets loaded with the electrolyte (i.e., 10 wt.% 62 Li_2CO_3:38 K_2CO_3). The hot reactant mixture flowed through the impregnated beads and then the catalyst bed. The reaction results for the Ni/Al_2O_3–Sil-1 core–shell catalyst are shown in Figs. 7a and b. During the 100 h reaction, the reactor outlet was monitored and the composition of the product gas remains unchanged at 63.0% H_2, 8.7% CO, 17.5% CO_2 and 19.0% CH_4 and the methane conversion of 50% and hydrogen yield of 20% are maintained. Fig. 7c shows Ni/Al_2O_3 loss activity with exposure to the electrolyte vapor, while the core–shell catalyst remained stable over the 120 h reaction study.

It is important to note that although the zeolite shell gave Ni/Al_2O_3–Sil-1 greater tolerance to alkali poisons from the DIR-MCFC electrolyte, the added transport resistance across the shell lead to lower activity compared to Ni/Al_2O_3 catalyst (Table 4). Fig. 8 plots methane conversion on fresh nickel catalysts with different Sil-1 shell thickness (Fig. 8a) and the effect of shell thickness on catalyst deactivation (Fig. 8b). The figures also show the results of model calculations of catalyst reaction and deactivation. The plots show that there is good agreement between experiment and model. The model correctly predicts the catalyst behavior during reaction and poisoning. The results show that thicker shell has lower initial methane conversion, but greater tolerance to the alkali poisons. The model calculations in Fig. 8c predicts that a shell thickness of 6.5 μm should be considered if the catalyst is to survive 240 h (i.e., 10 days) of operation under high alkali conditions following a failure of the anode barrier in a DIR-MCFC. The thickness was optimized to ensure less than 20% drop in methane conversion and hydrogen yield during the 240 h period (Table 5). However,

Table 5
Optimum zeolite shell thickness.

Total operation time (hr)	50	100	150	200	250
Optimal shell thickness (μm)	3	4	5	6	6.5
Time-averaged methane conversion (%)	53.0	44.3	38.9	34.9	31.9

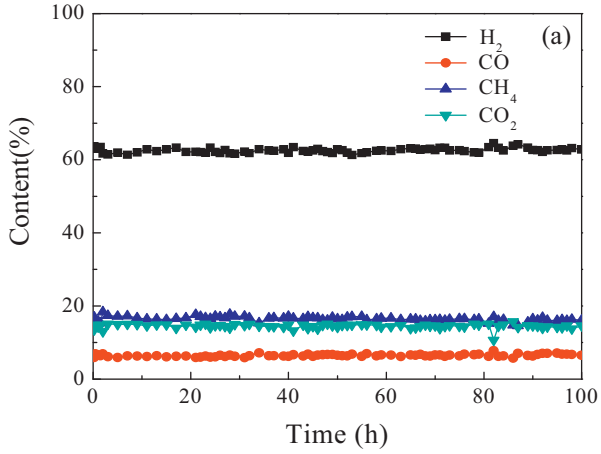

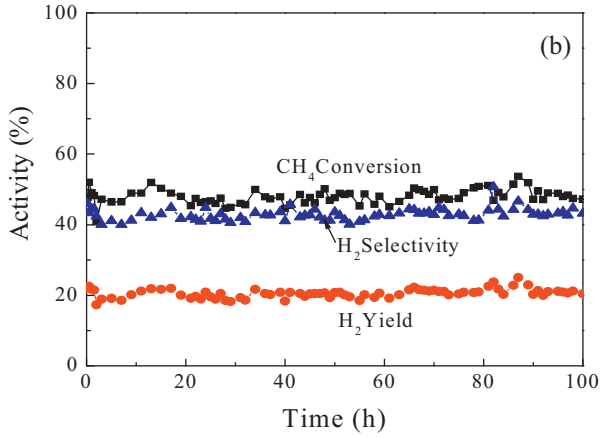

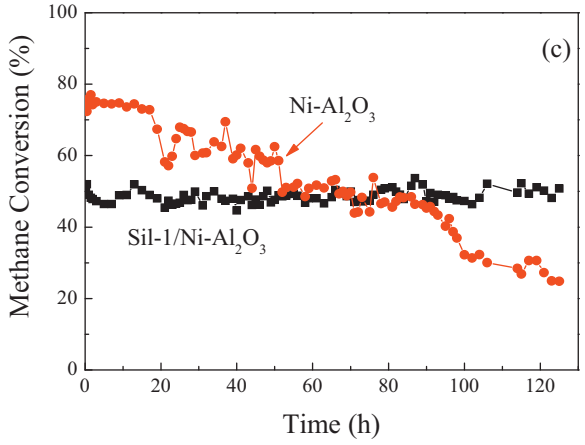

Fig. 7. Plots of (a) product composition and (b) catalytic activity of Ni/Al_2O_3–Sil-1 (3.5 μm) core–shell catalyst with time. (c) A comparison of catalyst activity between the nickel and nickel core–shell catalysts over 120 h reactions. *Note*: the methane steam reforming reaction was carried out at low concentration of electrolyte vapor to mimic normal DIR-MCFC operation.

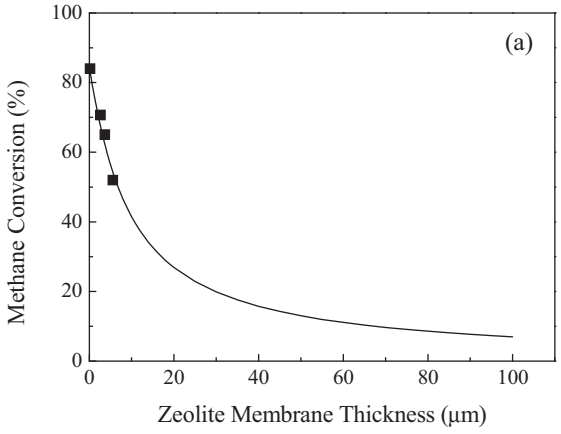

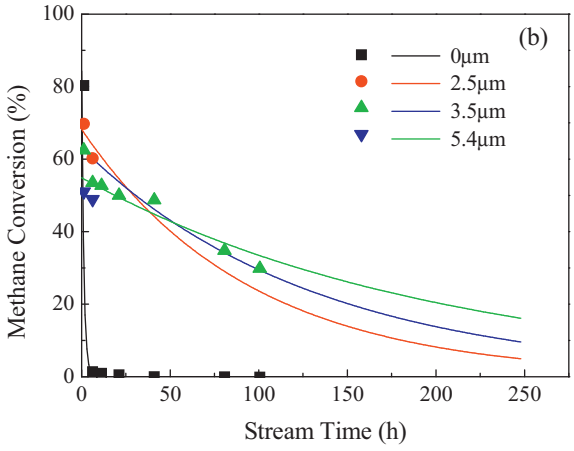

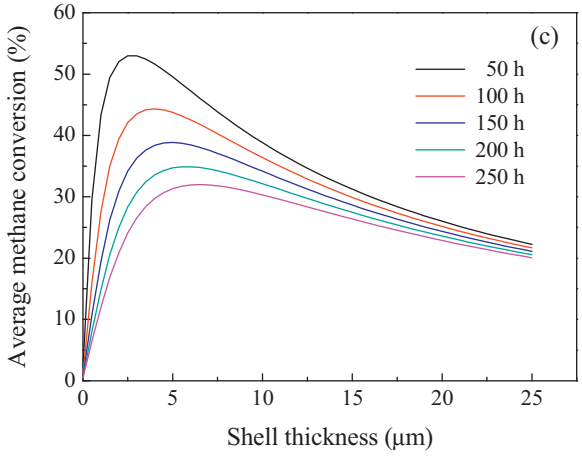

Fig. 8. Plots of methane conversion over (a) fresh nickel and nickel core–shell catalysts with different shell thicknesses, (b) nickel and nickel core–shell catalysts with time exposure to the electrolyte vapors, and (c) time-averaged methane conversion for different shell thickness after exposure to 50, 100, 150, 200 and 250 h exposure to the electrolyte vapor. Please note symbols denote experimental data and lines refer to mathematical modeling. (For interpretation of the references to color in this figure, the reader is referred to the web version of the article.)

66% more catalysts would be needed compared Ni/Al_2O_3 catalyst. A four micron thick shell similar to the core–shell catalyst shown in Figs. 6 would tolerate exposure to high alkali poisons for 100 h which would be sufficient time to institute repair and maintenance on the damaged DIR-MCFC.

3.3. *Post-reaction characterization of core–shell catalysts*

Fig. 9a–d is a series of pictures taken from Ni/Al_2O_3 and Ni/Al_2O_3–Sil-1 catalysts after exposure to electrolyte vapor. The poisoned Ni/Al_2O_3 catalyst bead has a dark blue coloration, while the core–shell catalyst exposed for the same length of time has a lighter coloration that progressively darken the longer it was exposed to the vapor. The blue coloration could be due to the formation Ni^{3+} species during exposure to alkali [51] (For interpretation of the references to color in this sentence, the reader is referred to the web version of the article.). It is also clear from Fig. 9c and d that that the surface of the catalyst beads assumed a darker coloration

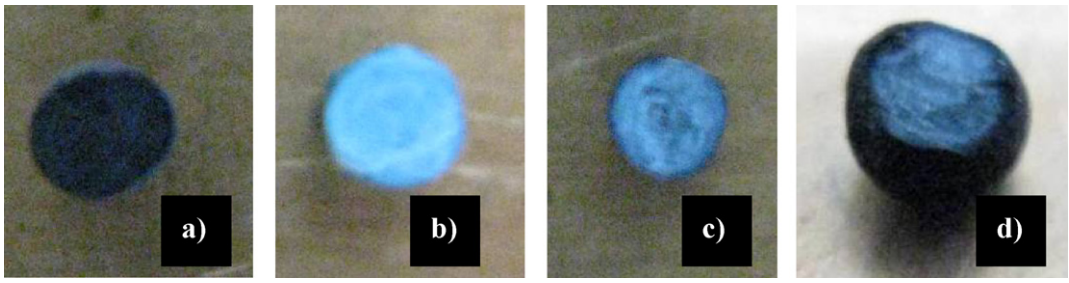

Fig. 9. Pictures of catalysts exposed to electrolyte vapor: (a) Ni/Al_2O_3 for 5 h and Ni/Al_2O_3–Sil-1 (3.5 μm) for (b) 5 h, (c) 50 h and (d) 100 h.

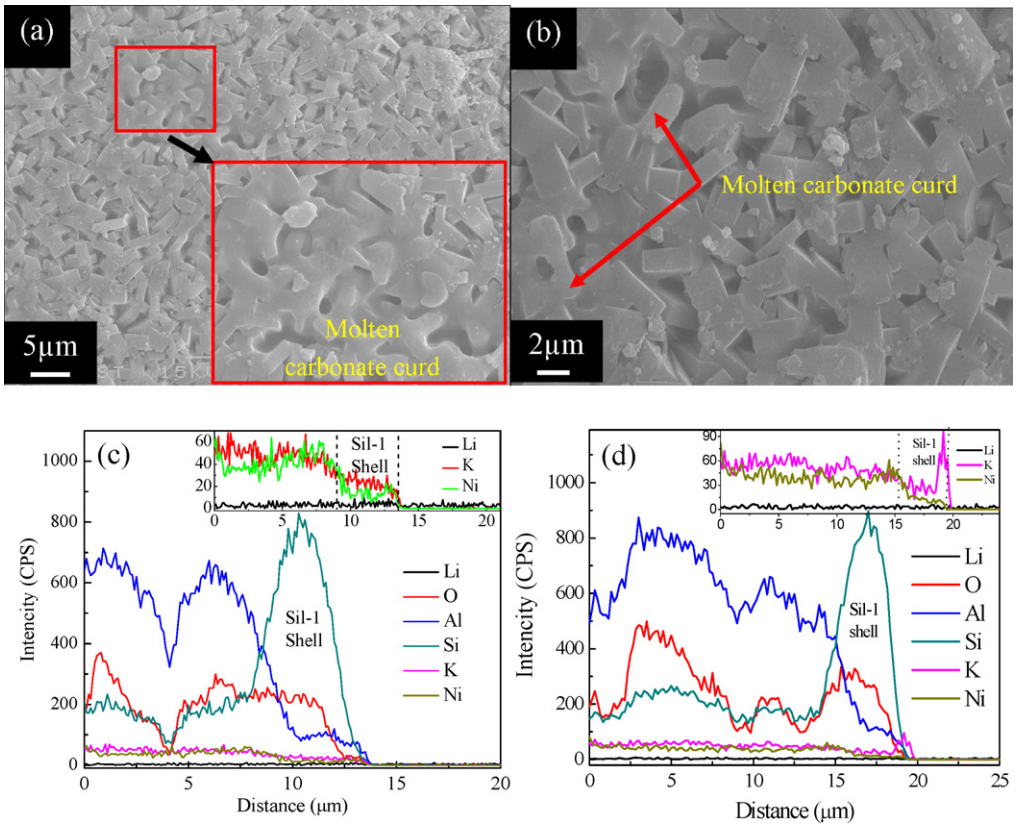

Fig. 10. SEM images of Ni/Al_2O_3–Sil-1 (3.5 μm) core–shell catalyst and the corresponding EDXS map of elemental composition along the catalyst diameter after exposure to the electrolyte vapor for (a and c) 5 h; (b and d) 100 h. (For interpretation of the references to color in this figure, the reader is referred to the web version of the article.)

(i.e., grey) than the catalyst interior. This strongly suggests that the zeolite shell is providing an effective barrier to the alkali poisons.

A closer examination of the shell surface (Fig. 10a and b) following 5 and 100 h exposure to the electrolyte vapor found evidence of solid electrolytes that could have condensed from the vapor and become physically trapped on the zeolite surface [9]. The composition along the core–shell catalysts was analyzed by energy dispersive X-ray spectroscopy and plotted in Fig. 10c and d. The elemental plots clearly show the thickness and location of the zeolite shell. It also showed that the nickel catalyst is uniformly dispersed on the alumina support. The zeolite shell contains a small amount of Al that were incorporated from the support during the zeolite regrowth. Surface enrichment of alkali on the shell surface is not apparent on short contact time (Fig. 10c inset), but is more evident after prolonged exposure (Fig. 10d inset). The weak signals from the alkalis are indicative of their low concentration in the catalyst. The spent catalysts were analyzed by ICP-AES and the poisoned Ni/Al_2O_3 catalysts contained 0.01 wt.% lithium and 0.03 wt.% potassium after 5 h treatment in electrolyte vapor. The core–shell catalysts treated for the same duration had elevated potassium content of 1.42 wt.% in agreement with observed electrolyte condensation on the catalyst shell. The lithium content (i.e., 0.01 wt.%) was comparable to the spent Ni/Al_2O_3. A 100 h exposure saw an increase in lithium content of 0.04 wt.%, but the potassium remained at 1.1 wt.%. This supports the EDXS and SEM observations that potassium was mainly deposited on the shell surface from the condensation electrolyte vapor.

4. Conclusion

Nickel core–shell catalysts prepared by depositing a thin zeolite shell on catalyst bead surface are shown to be effective against alkali poisoning from the molten carbonate electrolyte used in DIR-MCFC. The core–shell catalysts tolerate both low and high level exposure to the electrolyte vapor at the high temperatures encountered in DIR-MCFC operation. The catalysts maintained stable reaction performance under low exposure conditions expected under normal operating conditions and could slow deactivation in case of high

exposure caused by failure of anode barrier to afford sufficient time to institute repair and maintenance. However, the zeolite shell also increased transport resistant for the reactant resulting in lower conversion and thus requires more catalysts. It would be of interest to explore the possibility of mesoporous shells [52,53] to alleviate this shortcoming and the use of similar approach in other fuel cell systems [54,55].

Acknowledgements

We gratefully acknowledge the financial support by the National Natural Science Foundation of China (Grant No. 21036006, 21173030), China National 863 Program (Grant No. 2007AA05Z137) and Program for Liaoning Excellent Talents in University (Grant No. LR201008).

References

[1] B. Manfred, J. Power Sources 160 (2006) 842.
[2] V. Verda, F. Nicolin, Int. J. Hydrogen Energy 35 (2010) 794.
[3] M. Bischoff, G. Huppmann, J. Power Sources 105 (2002) 216.
[4] A.L. Dick, Curr. Opin. Solid State Mater. Sci. 8 (2004) 379.
[5] S. Katikaneni, C. Yuh, S. Abens, M. Farooque, Catal. Today 77 (2002) 99.
[6] S. Freni, S. Cavallaro, M. Aquino, D. Ravida, N. Giordano, Int. J. Hydrogen Energy 19 (1994) 337.
[7] S.H. Clarke, A.L. Dicks, K. Pointon, T.A. Smith, A. Swann, Catal. Today 38 (1997) 411.
[8] J.R. Rostrup-Nielsen, L.J. Christiansen, Appl. Catal. A 126 (1995) 381.
[9] E. Passalacqua, S. Freni, F. Barone, A. Patti, Mater. Lett. 29 (1996) 177.
[10] E. Passalacqua, S. Freni, F. Barone, Mater. Lett. 34 (1998) 257.
[11] L.G. Marianowski, Dual compartment anode structure, US: 4702973, 1987-10-27.
[12] T. Tagawa, M. Ito, S. Goto, Appl. Organomet. Chem. 15 (2001) 127.
[13] R.J. Berger, E.B.M. Doesburg, J.G. van Ommen, J.R.H. Ross, Appl. Catal. A: Gen. 143 (1996) 343.
[14] J.S. Choi, H.H. Kwon, T.H. Lim, S.A. Hong, H.-I. Lee, Catal. Today 93–95 (2004) 553.
[15] D.S. Park, Z.L. Li, H. Devianto, H.-I. Lee, Int. J. Hydrogen Energy 35 (2010) 5673.
[16] K.L. Yeung, A. Gavriilidis, A. Varma, M.M. Bhasin, J. Catal. 174 (1998) 1.
[17] K.L. Yeung, R. Aravind, R.J.X. Zawada, J. Szegner, G. Cao, A. Varma, Chem. Eng. Sci. 49 (1994) 4823.
[18] K.L. Yeung, J.M. Sebastian, A. Varma, J. Membr. Sci. 131 (1997) 9.
[19] K.L. Yeung, R. Aravind, J. Szegner, A. Varma, Stud. Surf. Sci. Catal. 101 (1996) 1349.
[20] J.J. He, Y. Yoneyama, B. Xu, N. Nishiyama, N. Tsubaki, Langmuir 21 (2005) 1699.
[21] N. Nishiyama, K. Ichioka, D.H. Park, Y. Egashira, K. Ueyama, L. Gora, W.D. Zhu, F. Kapteijn, J.A. Moulijn, Ind. Eng. Chem. Res. 43 (2004) 1211.
[22] K.L. Yeung, J.M. Sebastian, A. Varma, Catal. Today 25 (1995) 231.
[23] Y. Guo, X.F. Zhang, H.Y. Zou, H.O. Liu, J.Q. Wang, K.L. Yeung, Chem. Commun. (2009) 5898.
[24] Y. Guo, X.B. Wang, X.F. Zhang, Y. Wang, H.O. Liu, J.Q. Wang, J.S. Qiu, K.L. Yeung, Catal. Today 156 (2010) 282.
[25] X.B. Wang, Y. Guo, X.F. Zhang, Y. Wang, H.O. Liu, J.Q. Wang, J.S. Qiu, K.L. Yeung, Catal. Today 156 (2010) 288.
[26] J.L. Zhou, X.F. Zhang, J. Zhang, H.O. Liu, L. Zhou, K.L. Yeung, Catal. Commun. 10 (2009) 1804.
[27] J. Caro, M. Noack, Micropor. Mesopor. Mater. 115 (2008) 215.
[28] L.T.Y. Au, J.L.H. Chau, C.T. Ariso, K.L. Yeung, J. Membr. Sci. 183 (2001) 269.
[29] J.L.H. Chau, A.Y.L. Leung, K.L. Yeung, Lab Chip 3 (2003) 53.
[30] Y. Guo, X.F. Zhang, H.Y. Zou, H.O. Liu, J.Q. Wang, K.L. Yeung, Chem. Commun. 39 (2009) 5898.
[31] W.C. Wong, L.T.Y. Au, C. Tellez, K.L. Yeung, J. Membr. Sci. 191 (2001) 143.
[32] G.H. Yang, X.F. Zhang, S.Q. Liu, K.L. Yeung, J.Q. Wang, J. Phys. Chem. Solids 68 (2007) 26.
[33] J.L.H. Chau, C. Tellez, K.L. Yeung, K.C. Ho, J. Membr. Sci. 164 (2000) 257.
[34] S.M. Lai, L.T.Y. Au, K.L. Yeung, Micropor. Mesopor. Mater. 54 (2002) 63.
[35] N. Jiang, G.H. Yang, X.F. Zhang, L. Wang, C.Y. Shi, N. Tsubaki, Catal. Commun. 12 (2011) 951.
[36] L.T.Y. Au, K.L. Yeung, J. Membr. Sci. 194 (2001) 33.
[37] L.T.Y. Au, W.Y. Mui, P.S. Lau, C.T. Ariso, K.L. Yeung, Micropor. Mesopor. Mater. 47 (2001) 203.
[38] J.L.H. Chau, Y.S.S. Wan, A. Gavriilidis, K.L. Yeung, Chem. Eng. J. 88 (2002) 187.
[39] K. Ha, J.S. Park, K.S. Oh, Y.S. Zhou, Y.S. Chun, Y.J. Lee, K.B. Yoon, Micropor. Mesopor. Mater. 72 (2004) 91.
[40] S. Heng, P.P.S. Lau, K.L. Yeung, M. Djafer, J.C. Schrotter, J. Membr. Sci. 243 (2004) 69.
[41] J. Motuzas, S. Heng, P.P.S.Z. Lau, K.L. Yeung, Z.J. Beresnevicius, A. Julbe, Micropor. Mesopor. Mater. 99 (2007) 197.
[42] A.J. Bons, P.D. Bons, Micropor. Mesopor. Mater. 62 (2003) 9.
[43] A. Gouzinis, M. Tsapatsis, Chem. Mater. 10 (1998) 2497.
[44] C.H. Bartholomew, Appl. Catal. A: Gen. 212 (2001) 17.
[45] S. Takenake, Y. Tomikubo, E. Kato, K. Otsuka, Fuel 83 (2004) 47.
[46] R. Lai, Y. Yan, G.R. Gavalas, Micropor. Mesopor. Mater. 37 (2000) 9.
[47] R. Takahashi, S. Sato, T. Sodesawa, M. Yoshida, S. Tomiyama, Appl. Catal. A: Gen. 273 (2004) 211.
[48] H.S. Roh, K.W. Jun, W.S. Dong, J.S. Chang, S.E. Park, Y. Joe Il, J. Mol. Catal. A: Chem. 181 (2002) 137.
[49] F. Kapteijn, W.J.W. Bakker, J. van de Graaf, G. Zheng, J. Poppe, J.A. Moulijn, Catal. Today 25 (1995) 213.
[50] M.G. Ahunbay, J.R. Elliott, J.O. Talu, J. Phys. Chem. B 106 (2002) 5163.
[51] Z.L. Li, H. Devianto, S.P. Yoon, J.H. Han, T.H. Lim, H.-I. Lee, Int. J. Hydrogen Energy 35 (2010) 13041.
[52] M. Arruebo, W.Y. Ho, K.F. Lam, X.Q. Chen, J. Arbiol, J. Santamaria, K.L. Yeung, Chem. Mater. 20 (2008) 486.
[53] K.F. Lam, H. Kassab, M. Pera-Titus, K.L. Yeung, B. Albela, L. Bonneviot, J. Phys. Chem. C 116 (2011) 176.
[54] S.M. Kwan, K.L. Yeung, Chem. Commun. (2008) 3631.
[55] W. Han, K.L. Yeung, Chem. Commun. 47 (2011) 8085.